IRSTI 29.19.22, 29.19.31 https://doi.org/10.26577/phst20261317

Optimization of the carbon ink printing process for the fabrication of flexible printed perovskite optoelectronic devices

Ye. Yerlanuly[1,2] and A.N. Jumabekov[1,2,*]

[1]National Laboratory Astana, Astana, Kazakhstan;
[2]Department of Physics, School of Sciences and Humanities, Nazarbayev University, Astana, Kazakhstan
*e-mail: askhat.jumabekov@nu.edu.kz

(Received February 26, 2026; received in revised form April 30, 2026; accepted May 8, 2026)

Carbon-based electrodes represent a promising alternative to noble metals for fully printed flexible perovskite solar cells (FPSCs) due to their low cost, chemical stability, and compatibility with scalable manufacturing. In this work, the printing and optimization of carbon ink electrodes using slot-die coating and screen-printing techniques are systematically investigated for application in fully printed FPSCs. The influence of printing parameters on the electrical and structural properties of carbon films is evaluated through sheet resistance measurements and Raman spectroscopy. Slot-die-coated carbon electrodes deposited at an optimized pump rate of 1 mL min^{-1} exhibit uniform films with a sheet resistance of approximately 80 Ω sq^{-1}, while screen-printed electrodes fabricated using a multi-point paste application strategy show improved uniformity with an average sheet resistance of ~125 Ω sq^{-1}. Using the optimized electrodes, fully printed FPSCs with a regular (n–i–p) architecture are fabricated on PET substrates. Devices incorporating slot-die-coated carbon electrodes achieve a power conversion efficiency (PCE) of ~0.6% over a large active area, whereas screen-printed carbon electrodes enable improved performance with a maximum PCE of 3.86%. These results demonstrate the feasibility of low-temperature, vacuum-free fabrication of flexible perovskite solar cells and provide practical guidelines for scalable roll-to-roll manufacturing.

Key words: printed perovskite solar cells; carbon electrodes; slot-die coating; screen printing; flexible electronics

1. Introduction

Perovskite photovoltaics have attracted extraordinary scientific and technological interest over the past decade, driven by rapid and unprecedented improvements in device performance [1, 2]. Since the first reports of perovskite-based solar cells [3-6], their power conversion efficiency (PCE) has increased at an exceptional pace, now exceeding 27% at the laboratory scale [3–5]. Beyond these record efficiencies, a defining advantage of perovskite photovoltaics lies in their solution-processable nature, which enables low-temperature fabrication and opens a clear pathway toward scalable, cost-effective manufacturing, particularly via roll-to-roll (R2R) coating technologies [1, 6–10].

In this context, fully printed perovskite photovoltaic (PV) devices are considered one of the most promising pathways toward industrial-scale production. Among various scalable deposition techniques, slot-die coating has emerged as a leading candidate for R2R fabrication of perovskite optoelectronic devices due to its high material utilization, excellent thickness control, and compatibility with continuous processing [11–13]. Using benchtop and pilot-scale slot-die systems, notable progress has been demonstrated for both regular (n–i–p) and inverted (p–i–n) device architectures. Reported PCEs have reached approximately 13% for slot-die-coated n–i–p devices and around 12% for inverted p–i–n configurations based on triple-cation mixed-halide perovskites, highlighting the strong potential of this approach for scalable manufacturing [14, 15].

Despite substantial progress in coating perovskite absorber layers and charge transport layers, the final electrode deposition step remains a major bottleneck for fully printed and flexible perovskite devices. High-efficiency laboratory devices still predominantly rely on vacuum deposition of noble metals such as gold or silver, which is inherently time-consuming, expensive, and incompatible with high-throughput R2R processing. Although PCE values exceeding 18% have been reported using alternative low-cost electrodes, including carbon-based contacts, the widespread adoption of such approaches remains limited [16–30]. Many exist-

ing carbon electrode strategies depend on high-temperature sintering, mesoporous scaffolds, or complex multilayer designs, which are unsuitable for flexible polymer substrates and continuous R2R fabrication.

In recent years, increasing attention has been directed toward the development of printable conductive inks based on organic and inorganic materials for flexible electronics. Among these, conductive carbon inks have emerged as particularly attractive candidates for use in fully printed perovskite solar cells (PSCs) and other optoelectronic devices [25, 31,32]. Carbon-based electrodes offer several key advantages over conventional metal contacts, including low cost, excellent chemical stability, intrinsic resistance to ion migration, and mechanical robustness under bending. Moreover, carbon inks can be deposited using scalable printing techniques such as slot-die coating, screen printing, and blade coating, significantly reducing fabrication complexity and overall production costs. These attributes are especially critical for printed flexible perovskite solar cells (FPSCs), where lightweight, mechanically compliant, and environmentally stable components are essential for reliable operation.

Nevertheless, the performance of carbon-based electrodes in printed flexible perovskite devices is highly sensitive to ink formulation, rheological properties, printing parameters, and post-deposition treatment. Inadequate control over these factors often leads to poor film uniformity, high sheet resistance, weak adhesion, and suboptimal interfacial contact with underlying layers, ultimately limiting device efficiency and reproducibility. Therefore, systematic optimization of the carbon ink printing process is a crucial step toward realizing high-performance, fully printed, and flexible perovskite optoelectronic devices compatible with industrial R2R manufacturing.

This paper investigates the optimization of carbon ink printing processes based on slot-die coating and screen-printing techniques for the fabrication of flexible electrodes. The electrical performance of the printed carbon layers was systematically evaluated through sheet resistance measurements as a function of printing parameters and ink formulation. Furthermore, fully printed FPSCs were successfully fabricated using the optimized carbon electrodes, demonstrating their suitability for scalable, low-temperature, and roll-to-roll–compatible perovskite optoelectronic device manufacturing.

2. Materials and methods

2.1 Materials

All the chemicals and reagents were used as received without any further purification. A flexible polyethylene terephthalate (PET, thickness 125 μm) with a layer of patterned transparent conducting indium-tin-oxide (ITO, thickness 150 nm, and sheet resistance – 45 Ω sq^{-1}) was purchased from Mekoprint. SnO_2 nanoparticle (NP) based colloid dispersion (15 wt.% colloidal dispersion in H_2O) is purchased from Alfa Aesar. Methylammonium iodide (MAI, 99.995%) is purchased from GreatCell solar. Lead iodide (PbI_2, 99%), methylamine solution (MA, in absolute ethanol 33 wt.%), acetonitrile (ACN, 99.8%), chlorobenzene (CB, 99.8%), acetone (99.9%), and 2-propanol (IPA, 99.5%) are purchased from Merck. PEDOT complex purchased from Ossila. Carbon ink (DM-CAP-4701S) was purchased from Dycotec.

2.2 Device fabrication

To fabricate fully printed FPSCs, PET/ITO substrates were sequentially cleaned in an ultrasonic bath for 10 minutes each in deionized (DI) water with detergent, DI water, acetone, and IPA, then dried using a nitrogen gun. The cleaned substrates were subsequently treated with UV-ozone for 15 minutes to enhance surface wettability. The fabrication of fully printed FPSCs was carried out using slot-die coating techniques. A VectorSC sheet-to-sheet slot-die coater (FOM technologies, Denmark) was employed to deposit the electron transport layer (ETL) made of SnO_2 NPs and the top carbon electrode. For the deposition of the perovskite ($MAPbI_3$) layer and PEDOT complex-based hole transport layer (HTL), a NanoRoll slot-die coater (FOM technologies, Denmark) was used, with the process conducted inside a glove box to ensure a controlled environment.

The tin oxide ETL was prepared from a commercial SnO_2 NP-based colloidal dispersion solution, which was diluted with DI water at a volume ratio of 1:3. The SnO_2 layer was printed on cleaned PET/ITO substrates at 150 μL min^{-1} pump rate and 80 cm min^{-1} chuck speed at temperature 50 °C, followed by annealing on a hot plate at 130 °C for 30 minutes. After annealing, the substrates underwent an additional UV-ozone treatment for 30 minutes to further improve film quality and interfacial properties.

Next, the $MAPbI_3$ layer was printed using a pump rate of 0.15 mL min^{-1} and the same coating speed, then annealed at 100 °C for 10 minutes. The perovskite ink was prepared by dissolving 1 mol of MAI (159.3 mg) and PbI_2 (461 mg) in 700 μL of MA, stirring at 460 rpm at 70°C for one hour. Afterward, 700 μL of ACN was added, and the solution was stirred at room temperature for 3 hours. The perovskite layer was coated at a pump rate of 70 μL min^{-1} and a chuck speed of 70 cm min^{-1} at a temperature of 130 °C. The films were then annealed on a hot plate at 100 °C for

10 minutes and allowed to cool to room temperature. Following the perovskite deposition, the PEDOT layer was applied under the same conditions as the perovskite layer. One sample was annealed at 100 °C for 10 minutes, while another was left unannealed.

The top carbon electrode was optimized and deposited using two methods: slot-die coating and screen-printing techniques.

2.3 Materials and device characterizations

The sheet resistance of electrodes was measured using a four-point system (RM3000, Jandel, UK). Raman Spectroscopy (Horiba LabRam Evolution) was used for structural characterization of carbon electrodes. A semiconductor device analyzer (B1500A, Keysight, USA) coupled with a 3A+ solar simulator (Oriel Sol3A, Newport, USA) providing an AM 1.5G illumination intensity of 100 mW cm^{-2} was used to measure the *J-V* characteristics of the devices.

3. Results and discussion

3.1 Optimization of carbon ink printing

First, experiments were carried out to evaluate the application of carbon ink (0.5 g in 1 mL of CB) and its electrical properties at varying pump rates (0.5-1 mL min^{-1}). The application speed was set at 0.8 m s^{-1}, and after the carbon film was deposited onto the PET substrate, the samples were annealed at 100 °C for 30 minutes to optimize film quality and ensure proper conductivity. Figure 1a shows a schematic sketch of the PET substrate used, displaying the numbering of the sections along the length of the substrate. Figure 1b displays a photographic image of the slot-die coating of a carbon film on top of a PET substrate. The carbon films were deposited at pump rates of 0.5, 0.75, and 1 mL min^{-1} (see Figures 1c and 1d). The results demonstrate that as the pump rate increases, sheet resistance decreases, which is attributed to the thicker carbon films produced with higher pump rates. Notably, at a pump rate of 1 mL min^{-1}, the carbon film exhibited a more uniform sheet resistance (~80 Ω sq^{-1}) compared to other pump rates, suggesting that this parameter offers a better consistency in film conductivity across the substrate (Figure 1c). This uniformity is crucial for improving the overall performance and reliability of devices.

The results indicate a clear inverse relationship between pump rate and sheet resistance. Although higher pump rates could potentially yield even lower resistance values, excessive ink supply may cause film inhomogeneity or ink overflow beyond the intended coating area. Based on these considerations, the optimized slot-die coating and annealing parameters for carbon electrode fabrication are summarized in Table 1.

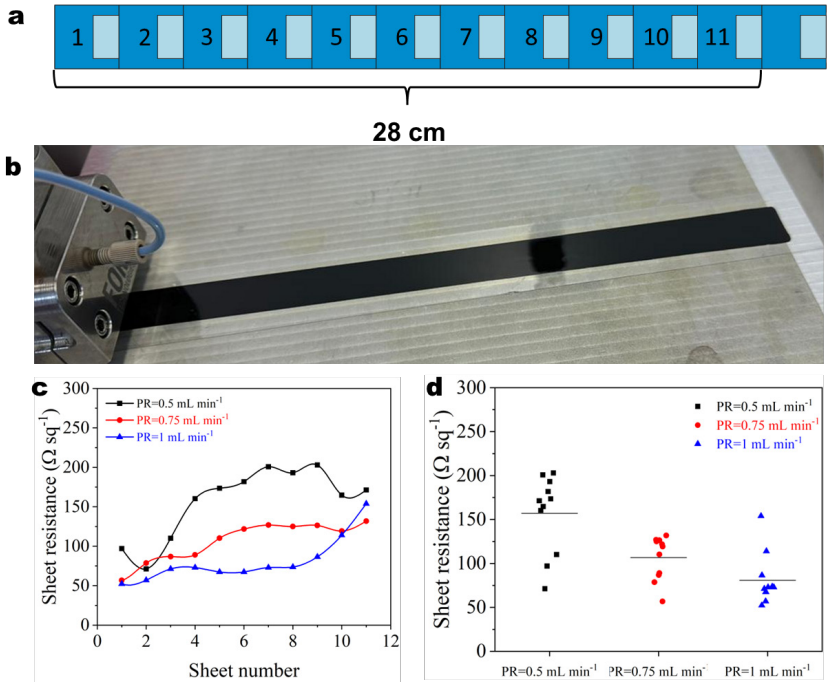

Figure 1. Sheet resistance of slot-die-coated carbon films on PET substrates at different pump rates (PR). a) Schematic of PET substrate section numbering for sheet resistance mapping. b) Photograph of a representative slot-die-coated carbon stripe on PET. c) Sheet resistance distribution along the substrate at PR = 0.5, 0.75, and 1.0 mL min^{-1}. d) Statistical comparison of sheet resistance at different PR.

Table 1. Optimal slot-die coating and annealing parameters for the carbon films on PET.

Coating parameters	Carbon
Chuck temperature (°C)	25
Coating speed (cm min^{-1})	80
Pump rate (mL min^{-1})	1
Coating window (μm)	221
Annealing temperature (°C)	100
Annealing time (min)	30

For the screen-printing process, a PET substrate was positioned beneath the patterned screen of the screen printer, which defined the electrode geometry. A controlled amount of carbon paste was then deposited onto the screen and transferred onto the PET substrate by sweeping a squeegee across the screen under uniform pressure, ensuring reproducible electrode formation. After printing, the screen was lifted, and the PET substrates with the printed carbon electrodes were annealed on a vacuum hot plate at 100 °C for 30 minutes to enhance film adhesion and electrical conductivity.

Two different electrode deposition strategies were investigated, as schematically illustrated in Figures 2a and 2b. In the first approach (Type 1), the carbon paste was applied at a single point along the screen (Figure 2a). In contrast, the second approach (Type 2) employed multi-point paste application along the printing direction to improve ink distribution (Figure 2b). As shown in Figure 2c, the single-point method resulted in non-uniform carbon electrode deposition, featuring thickness variations and incomplete coverage. In comparison, the multi-point method produced more homogeneous and continuous carbon films across the substrate.

The corresponding sheet resistance measurements are presented in Figures 2d and 2e. The electrodes fabricated using the multi-point printing strategy consistently exhibited lower sheet resistance values compared to those produced by the single-point method. The average sheet resistance of the optimized screen-printed carbon electrodes was approximately 125 Ω sq^{-1}. Owing to its superior film uniformity and electrical performance, the multi-point screen-printing method was selected for subsequent fabrication of fully printed FPSCs.

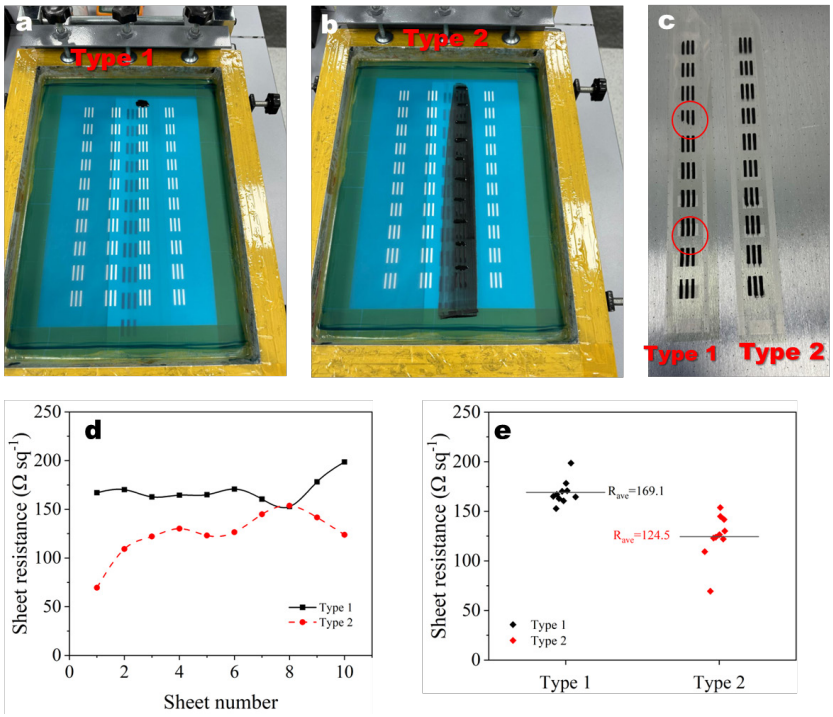

Figure 2. Comparison of carbon electrode deposition methods: single-point (Type 1) and multi-point (Type 2) screen printing. a) Screen-printing setup using single-point carbon paste application (Type 1). b) Screen-printing setup using multi-point carbon paste application (Type 2). c) Photograph of printed carbon electrode patterns obtained by Type 1 and Type 2. d) Sheet resistance distribution along the printed electrodes for Type 1 and Type 2. e) Statistical comparison of sheet resistance.

Figure 3 presents the Raman spectra of printed carbon films fabricated using two different coating techniques: slot-die coating and screen printing. The spectra exhibit characteristic features of carbon materials, including the D band (~1350 cm^{-1}), which is associated with structural disorder, and the G band (~1580 cm^{-1}), corresponding to graphitic sp^2-bonded carbon. Additional features, such as the D′ peak and the 2D band, provide further insight into the structural integrity and degree of graphitization of the films. The overall similarity of the Raman spectra indicates that the carbon films possess comparable structural properties, irrespective of the coating method employed.

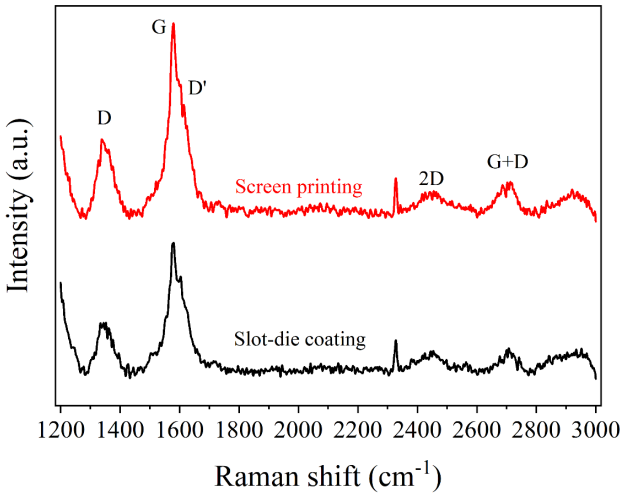

Figure 3. Raman spectra of printed carbon films on PET fabricated using different coating techniques.

Overall, both fabrication techniques – slot-die coating and screen printing – were effective to varying degrees, although the resulting electrodes exhibited different levels of conductivity. The lowest sheet resistance was obtained for the slot-die-coated electrodes, while the screen-printed electrodes exhibited higher sheet resistance. Nevertheless, screen printing offers a clear advantage in enabling the fabrication of small electrodes with well-defined and precise geometries required for device integration. Raman spectroscopy revealed comparable structural characteristics for the printed carbon electrodes, indicating that the coating method has a negligible impact on the intrinsic carbon structure.

3.2 Fabrication of fully printed flexible perovskite solar cells

Fully printed FPSCs incorporating printed carbon top electrodes were fabricated using optimized carbon printing parameters. All devices employed a regular (n–i–p) architecture, schematically illustrated in Figure 4a. The fabrication of fully printed FPSCs was carried out using slot-die coating techniques. The device architecture and corresponding layer thicknesses are as follows: PET (125 μm)/ITO (~150 nm)/SnO_2 ETL (~10 nm)/$MAPbI_3$ perovskite (~400 nm)/PEDOT HTL (~100 nm)/carbon electrode (~30–50 μm depending on deposition method). The thickness of the carbon electrode depends on the deposition technique, being ~40 μm for slot-die coating and ~30–50 μm for screen printing. Due to the inherent surface roughness and non-uniformity of printed carbon films, precise thickness determination is challenging, and profilometry measurements showed significant spatial variation.

Two types of fully printed FPSCs were prepared, distinguished by the carbon electrode deposition method. In the first configuration, a single-layer slot-die-coated carbon (C_{SDC}) electrode was employed as the top contact, yielding a PET/ITO/SnO_2/$MAPbI_3$/PEDOT/C_{SDC} device structure. In the second configuration, a single-layer screen-printed carbon (Indicate Type 2 C_{SP}) electrode served as the top contact, resulting in a similar PET/ITO/SnO_2/$MAPbI_3$/PEDOT/C_{SP} device structure.

Photographic images of the fabricated flexible devices are shown in Figures 4b and 4c. Figure 4b presents a representative fully printed FPSC with a continuous carbon top electrode, demonstrating good coverage and mechanical flexibility of the device. Figure 4c shows a flexible device with patterned printed carbon electrodes, highlighting the compatibility of the developed printing processes with electrode patterning and flexible substrate handling. These results demonstrate a successful integration of printed carbon electrodes into fully printed FPSCs.

Figure 5 displays the *J-V* curve of the best-performing fully printed FPSC with a C_{SDC} top electrode, along with statistical data for the photovoltaic parameters of ten devices. The active area of the devices was 1.95 cm^2. The results indicate that devices with C_{SDC} top electrodes demonstrate moderate performance, with the best-performing device achieving a PCE of approximately 0.6%. In addition, the

series resistance (Rs) of the devices was extracted and is presented in Figures 5f. The observed Rs values correlate well with the sheet resistance of the carbon electrodes, confirming that electrode conductivity plays a key role in charge transport and device performance. The main performance-limiting factors for these devices are attributed to low J_{SC} and FF, primarily due to the large active area and the low conductivity of the single-layer C_{SDC}. By reducing the active area and depositing multiple layers of C_{SDC}, it may be possible to achieve improved device performance.

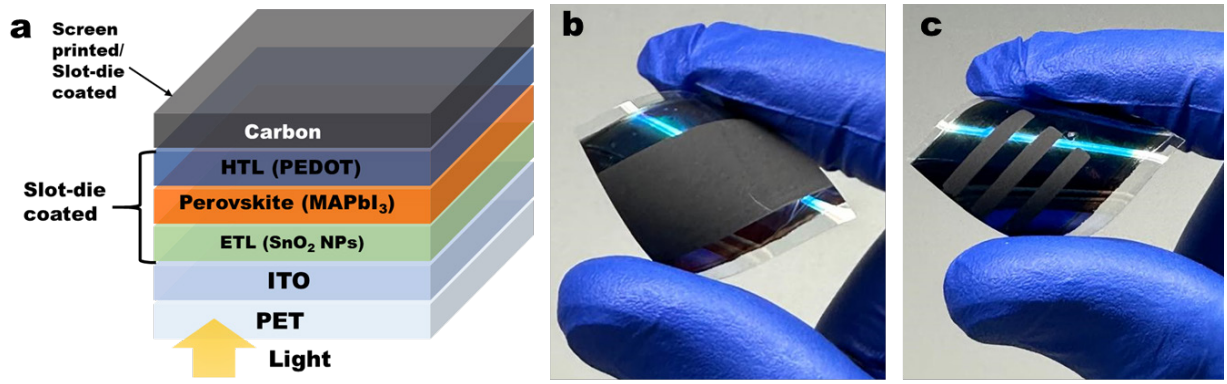

Figure 4. Schematic illustration of the FPSC device structure and photographic images of fully printed FPSCs fabricated with printed carbon electrodes. a) Schematic illustration of the n–i–p device structure. b) Photograph of a fully printed FPSC fabricated using the slot-die coating method. c) Photograph of a fully printed FPSC with screen-printed carbon electrodes.

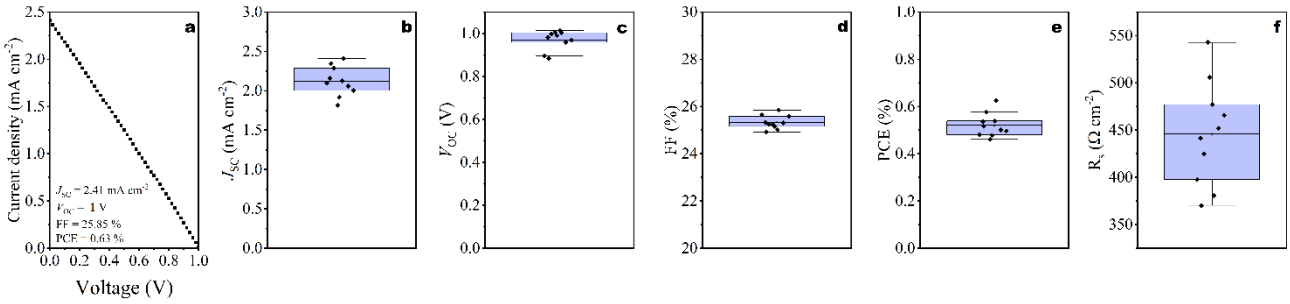

Figure 5. Solar cell performance results of fully printed FPSCs with C_{SDC} top electrodes. a) *J-V* curve of the best-performing device and statistical data for b) J_{SC}, c) V_{OC}, d) FF, e) PCE, and series resistance (Rs) of fully printed FPSCs with C_{SDC} top electrodes.

Figure 6 displays the *J-V* curve of the best-performing fully printed FPSC with a C_{SP} top electrode, along with statistical data for the photovoltaic parameters of twenty devices. The active area of the completed devices was 0.15 cm^2. The results indicate that devices with C_{SP} top electrodes exhibit improved performance, achieving a PCE of approximately 3.86%. In addition, the series resistance (Rs) of the devices was extracted and is presented in Figures 6f. The observed Rs values correlate well with the sheet resistance of the carbon electrodes, confirming that electrode conductivity plays a key role in charge transport and device performance. The main performance-limiting factor in this case is attributed to the low FF, which results from the low conductivity of the C_{SP}. Nevertheless, this represents a significant improvement compared to the devices with C_{SDC} (see Figure 5). Increasing the thickness of the C_{SP} holds promise for further enhancing device performance.

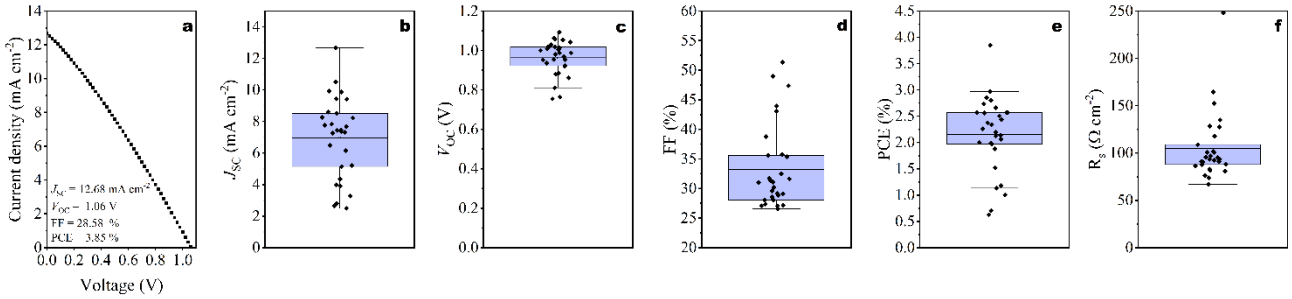

Figure 6. Solar cell performance results of fully printed FPSCs with C_{SP} top electrodes. a) *J-V* curve of the best-performing device and statistical data for b) J_{SC}, c) V_{OC}, d) FF, e) PCE, and series resistance (Rs) of fully printed FPSCs with C_{SP} top electrodes.

Overall, these results indicate that further performance enhancement of fully printed FPSCs with carbon top electrodes critically depends on optimizing the electrode morphology, electrical conductivity, and interfacial contact quality. This finding highlights the decisive role of carbon electrode deposition in governing the overall device performance of fully printed FPSCs.

In addition to the electrode-related limitations discussed above, the overall device performance is further constrained by interfacial and material-related factors. In particular, the HTL/carbon interface represents a critical bottleneck due to imperfect physical contact, surface roughness, and the absence of interfacial passivation, which can promote non-radiative recombination and hinder efficient charge extraction. These effects contribute to increased series resistance and reduced fill factor. Furthermore, the use of $MAPbI_3$ as the perovskite absorber introduces intrinsic limitations in terms of defect density and optoelectronic quality, resulting in lower achievable efficiencies compared to state-of-the-art multi-cation and mixed-halide perovskites.

To address these challenges, several strategies can be considered. The incorporation of interfacial passivation layers between the HTL and the carbon electrode could suppress recombination losses and improve energy level alignment. In addition, post-deposition treatments such as mechanical pressing or pulsed light annealing may enhance the physical contact and electrical connectivity at the interface. Finally, the implementation of more advanced perovskite compositions with improved crystallinity and reduced defect density is expected to significantly enhance device performance. These approaches provide a clear pathway toward improving the efficiency of fully printed FPSCs.

4. Conclusion

In this work, carbon-based electrodes for fully printed flexible perovskite solar cells were fabricated and optimized using two scalable printing techniques: slot-die coating and screen-printing. The influence of printing parameters on the electrical performance and uniformity of the carbon films was systematically investigated, followed by their integration into fully printed n–i–p perovskite device structure.

Slot-die-coated carbon electrodes exhibited a clear decrease in sheet resistance with increasing pump rate, with an optimized condition of 1 mL min^{-1} yielding uniform films with a sheet resistance of ~80 Ω sq^{-1} after low-temperature annealing. For screen-printed electrodes, a multi-point paste application strategy significantly improved film uniformity and reduced sheet resistance to ~125 Ω sq^{-1} compared to single-point deposition. Raman spectroscopy confirmed comparable structural properties of the carbon films produced by both methods, indicating that electrical differences mainly arise from film morphology and thickness.

Using the optimized electrodes, two types of fully printed FPSCs were fabricated. Devices with single-layer slot-die-coated carbon (C_{SDC}) top electrodes achieved a maximum PCE of ~0.6% over a large active area (1.95 cm^2), while devices employing screen-printed carbon (C_{SP}) electrodes reached a higher PCE of up to 3.86% for smaller-area devices (0.15 cm^2). The improved performance of CSP-based devices is attributed to enhanced charge collection resulting from thicker and more conductive carbon contacts.

Overall, this study demonstrates the feasibility of fully printed, flexible perovskite solar cells employing carbon-based top electrodes without vacuum processing. Further improvements are expected through

increasing carbon electrode thickness, enhancing conductivity, and optimizing interfacial contact, paving the way toward scalable, roll-to-roll fabrication of flexible perovskite optoelectronic devices.

Funding

Science Committee of the Ministry of Science and Higher Education of the Republic of Kazakhstan (grant numbers AP26194151).

Acknowledgements

We would like to thank the Core Facilities team of Nazarbayev University.

Conflicts of interest

The authors declare no conflict of interest.

Author contributions.

Conceptualization: Y.Y. and A.N.J.; Methodology Y.Y. and A.N.J.; Validation Y.Y.; Formal Analysis, Y.Y. and A.N.J.; Investigation, Y.Y. and A.N.J.; Resources, Y.Y. and A.N.J.; Data Curation, Y.Y.; Writing – Original Draft Preparation, Y.Y; Writing – Review & Editing, A.N.J..; Visualization, Y.Y.; Supervision, A.N.J.; Project Administration, Y.Y.; Funding Acquisition, Y.Y."

References

1. Y. Jung, K. Hwang, Y. Heo, J. Kim, D. Vak, D. Kim. "Progress in scalable cating and roll-to-roll compatible printing processes of perovskite solar cells toward realization of commercialization". *Adv. Opt. Mater*., vol.6, no. 11, Art. no. 1701182, 2018. https://doi.org/10.1002/adom.201701182.

2. T. Webb, S.J. Sweeney, W. Zhang, "Device architecture engineering: progress toward next generation perovskite solar cells", *Adv. Funct. Mater*., vol. 31, no 35, p. 2103121, 2021. https://doi.org/10.1002/adfm.202103121.

3. https://www.nrel.gov/pv/cell-efficiency.html .

4. A. Ghosh, A. Bakkar, Momina et al., "Enhancing solar cell efficiency beyond 27% through the implementation of an efficient charge transport layer utilizing an innovative inorganic perovskite Sr3PI3", *Journal of Physics and Chemistry of Solids,* vol.190, Art. no.112029, 2024. https://doi.org/10.1016/j.jpcs.2024.112029.

5. Z. Xiong, Q. Zhang, K. Cai et al., "Homogenized chlorine distribution for PCE;27% power conversion efficiency in perovskite solar cells", *Science*, vol. 390, no. 6773, pp.638–642, 2025. https://doi.org/10.1126/science.adw8780.

6. D. Beynon, E. Parvazian, K. Hooper et al., "All-printed roll-to-roll perovskite photovoltaics enabled by solution-processed carbon electrode", *Advanced Materials,* vol. 35, no. 16, Art. no.2208561, 2023. https://doi.org/10.1002/adma.202208561.

7. T.M. Schmidt, T.T. Larsen-Olsen, J.E. Carlé, D. Angmo, F.C. vKrebs, "Upscaling of perovskite solar cells: fully ambient roll processing of flexible perovskite solar cells with printed back electrodes", *Adv. Energy Mater.,* vol. 5, no. 15, Art. no. 1500569, 2015. https://doi.org/10.1002/aenm.201500569.

8. A.H. Ghahremani, T. Druffel, "Realizing perovskite solar cells on roll roll-to-roll compatible processes", in: 2019 IEEE 46th Photovoltaic Specialists Conference (PVSC), IEEE,: pp. 1–5, 2019. https://doi.org/10.1109/PVSC40753.2019.9198957.

9. A. Dyadenchuk, O. Roman, Y. Kuris, "Structural and electrical characteristics of the ZnO/porous-Si/Si heterostructure: from synthesis to analysis of photocell efficiency", *Int. J. of Math. and Phys.*, vol. 15, no. 2, pp. 34–41, 2024. https://doi.org/10.26577/ijmph.2024v15i2b4.

10. A.T. Sultanov, I. Zhirkov, A. Suleimenova, N. Beisenkhanov, "Computer simulation of planar bifacial TOPCon solar cells by using Quokka 3 software", *Physical Sciences and Technology*, vol. 12, no. 3-4, pp.93–105, 2025. https://doi.org/10.26577/phst20251229.

11. D. Burkitt, R. Patidar, P. Greenwood et al., "Roll-to-roll slot-die coated P–I–N perovskite solar cells using acetonitrile based single step perovskite solvent system", *Sustain. Energy Fuels*, vol.4, no. 7, pp. 3340–3351, 2020. https://doi.org/10.1039/D0SE00460J.

12. Y.Y. Kim, T.-Y. Yang, R. Suhonen, A. Kemppainen, K. Hwang, N.J. Jeon, J. Seo, "Roll-to-roll gravure-printed flexible perovskite solar cells using eco-friendly antisolvent bathing with wide processing window", *Nat. Commun.*, vol.11, Art. no. 5146, 2020. https://doi.org/10.1038/s41467-020-18940-5.

13. J. Kim, S. Kim, C. Zuo, M. Gao, D. Vak, D. Kim, "Humidity-tolerant roll-to-roll fabrication of perovskite solar cells via polymer-additive-assisted hot slot die deposition", *Adv. Funct. Mater.,* vol.29, no.29, Art. no.1809194, 2019. https://doi.org/10.1002/adfm.201809194.

14. H. Li, C. Zuo, D. Angmo, H. Weerasinghe, M. Gao, J. Yang, "Fully roll-to-roll processed efficient perovskite solar cells via precise control on the morphology of PbI_2:CsI layer", *Nanomicro Lett.,* vol.14, Art. no. 79, 2022. https://doi.org/10.1007/s40820-022-00815-7.

15. M. Othman, F. Zheng, A. Seeber et. al., "Millimeter-sized clusters of triple cation perovskite enables highly efficient and reproducible roll-to-roll fabricated inverted perovskite solar cells", *Adv. Funct. Mater.,* vol. 32, no. 12, Art. no. 2110700, 2022. https://doi.org/10.1002/adfm.202110700.

16. Z. Gu, L. Zuo, T.T. Larsen-Olsen, T. Ye, G. Wu, F.C. Krebs, H. Chen, "Interfacial engineering of self-assembled monolayer modified semi-roll-to-roll planar heterojunction perovskite solar cells on flexible substrates", *J. Mater. Chem. A Mater*., vol. 3, pp. 24254–24260, 2015. https://doi.org/10.1039/C5TA07008B.

17. F. Bisconti, A. Giuri, R. Suhonen et.al., "One-step polymer assisted roll-to-roll gravure-printed perovskite solar cells without using anti-solvent bathing", *Cell Rep. Phys. Sci*., vol. 2, no. 11, Art. no. 100639, 2021. https://doi.org/10.1016/j.xcrp.2021.100639.

18. L.J. Sutherland, D. Vak, M. Gao, T.A.N. Peiris, J. Jasieniak, G.P. Simon, H. Weerasinghe, "Vacuum-free and solvent-free deposition of electrodes for roll-to-roll fabricated perovskite solar cells", *Adv. Energy Mater.*, vol. 12, no. 40, Art. no. 2202142, 2022. https://doi.org/10.1002/aenm.202202142.

19. J.F. Benitez-Rodriguez, D. Chen, et.al., "Slot-die coating of a formamidinium-cesium mixed-cation perovskite for roll-to-roll fabrication of perovskite solar cells under ambient laboratory conditions", *Solar Energy Materials and Solar Cells*, vol. 246, Art. no. 111884, 2022. https://doi.org/10.1016/j.solmat.2022.111884.

20. A.G. Kakimov, Y. Yerlanuly, A. Akhanuly, et. al., "Passivation of perovskite layer surface states with pyridine in flexible and printed perovskite solar cells", *Flexible and Printed Electronics*, vol. 7, Art. no. 035012, 2022. https://doi.org/10.1088/2058-8585/ac8753.

21. M.S. Kiani, Z.T. Sadirkhanov, A.G. Kakimov, H.P. Parkhomenko, A. Ng, A.N. Jumabekov, "Solution-processed sno2 quantum dots for the electron transport layer of flexible and printed perovskite solar cells", *Nanomaterials*, vol. 12, no.15, Art. no. 2615, 2022. https://doi.org/10.3390/nano12152615.

22. M.S. Kiani, H.P. Parkhomenko, M. Mangrulkar, et. al., "Stepping toward portable optoelectronics with sno $_2$ quantum dot-based electron transport layers", *ACS Omega*, vol. 8, no. 23, pp.21212–21222, 2023. https://doi.org/10.1021/acsomega.3c02341.

23. H. Wang, F. Yang, X. Li, P. Zhang, "Fully printed high-performance quasi-two-dimensional perovskite solar cells via multifunctional interfacial engineering", *Adv. Funct. Mater*., vol. 34, no.10, Art. no. 2312250, 2024. https://doi.org/10.1002/adfm.202312250.

24. H.P. Parkhomenko, Y. Yerlanuly, V. V. Brus, A.N. Jumabekov, "Effect of mild mechanical stresses on device physics of slot-die coated flexible perovskite solar cells", *Org. Electron*., vol. 129, Art. no. 107049, 2024. https://doi.org/10.1016/j.orgel.2024.107049.

25. H.C. Weerasinghe, N. Macadam, J.-E. Kim, et al., "The first demonstration of entirely roll-to-roll fabricated perovskite solar cell modules under ambient room conditions", *Nat. Commun*., vol. 15, Art. no. 1656, 2024. https://doi.org/10.1038/s41467-024-46016-1.

26. L.J. Sutherland, J. Benitez-Rodriguez, D. Vak, et. al., "A high-pressure isostatic lamination technique to fabricate versatile carbon electrode-based perovskite solar cells", *Commun. Mater.,* vol. 5, Art. no. 90, 2024. https://doi.org/10.1038/s43246-024-00530-3.

27. V. Messerle, A. Ustimenko, "Plasmatron with renewable carbon nanostructured covering of electrodes", *Physical Sciences and Technology*, vol. 1, no.1, pp. 43–47, 2014. https://doi.org/10.26577/phst-2014-1-13.

28. A. Malgazhdarova, M. Kazankapova, B. Yermagambet, et. al., "Synthesis and characterization of carbon nanomaterials obtained using electric discharge", *Physical Sciences and Technology*, vol. 12, no. 1-2, pp. 68–83, 2025. https://doi.org/10.26577/phst20251217.

29. Sh.T. Nurbolat, M. Gabdullin, Zh. Kalkozova, M. Mirzaeian, Kh. Abdullin, "Capacitive electrodes based on a combination of activated carbon and graphene", *Physical Sciences and Technology*, vol. 9, no. 3-4, pp. 18–24, 2022. https://doi.org/10.26577/phst.2022.v9.i2.03.

30. Zh.A. Kudyshev, I.R. Gabitov, A. Kissan, Ye.S. Mukhametkarimov, "Hyperbolic metamaterials based on graphene sheets with different values of chemical potentials", *Physical Sciences and Technology*, vol. 3, no. 2, pp. 4–11, 2016. https://doi.org/10.26577/phst-2016-2-100.

31. N. Mussakhanuly, Y. Yerlanuly, H.P. Parkhomenko, A. Niyetullayeva, A.K. Azamat, A. Sultanov, Z. Kukhayeva, A. Ng, A.N. Jumabekov, "Laminated carbon based flexible printed perovskite solar cells passivated with tin(ii) phthalocyanine", *Adv. Mater. Interfaces*, vol. 12, no. 5, Art. no. 2400591, 2025. https://doi.org/10.1002/admi.202400591.

32. S.L. Mikhailova, O.Yu. Prikhodko, N.K. Manabaev, "Electrical properties of a-C:H films modified by Pt", *International Journal of Mathematics and Physics*, vol.5, no. 2, pp. 64–67, 2014. https://doi.org/10.26577/2218-7987-2014-5-2-64-67.

Information about authors:

Yerassyl Yerlanuly – PhD, Senior researcher, National Laboratory Astana, Department of Physics, School of Sciences and Humanities, Nazarbayev University (Astana, Kazakhstan, email: yerassyl.yerlanuly@nu.edu.kz);

Askhat N. Jumabekov (corresponding author) – Dr. rer. Nat. (PhD), Associate Professor of the Department of Physics, School of Sciences and Humanities, Nazarbayev University (Astana, Kazakhstan, email: askhat.jumabekov@nu.edu.kz).